iScience, Volume *23*

Supplemental Information

Trans-omic Analysis Reveals ROS-Dependent Pentose Phosphate Pathway Activation after High-Frequency Electrical Stimulation in C2C12 Myotubes

Daisuke Hoshino, Kentaro Kawata, Katsuyuki Kunida, Atsushi Hatano, Katsuyuki Yugi, Takumi Wada, Masashi Fujii, Takanori Sano, Yuki Ito, Yasuro Furuichi, Yasuko Manabe, Yutaka Suzuki, Nobuharu L. Fujii, Tomoyoshi Soga, and Shinya Kuroda

Supplemental Information

Supplemental figures

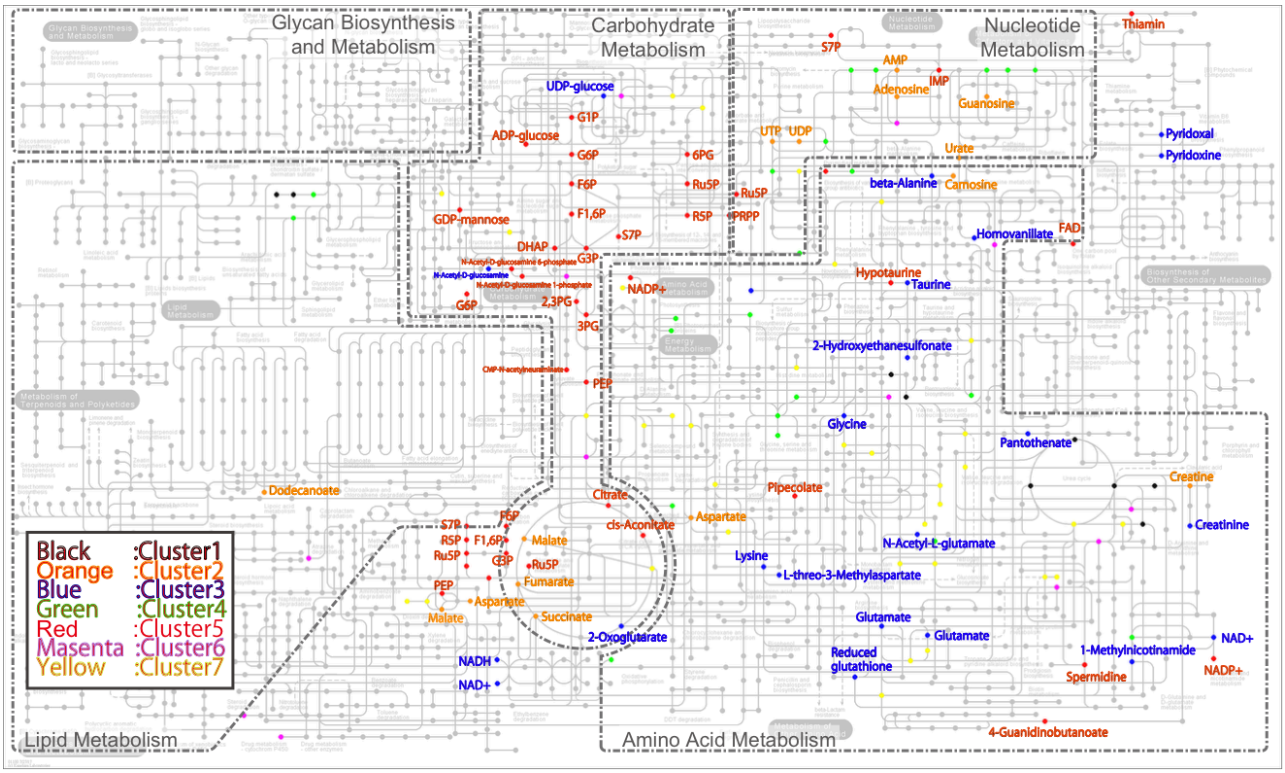

Figure S1 - The measured metabolites in each cluster were mapped on the KEGG global metabolism map. Names colored in orange, blue, and red correspond to metabolites in clusters 2, 3, and 5 in Fig 2, respectively. Related to Figure 2 and 3.

A

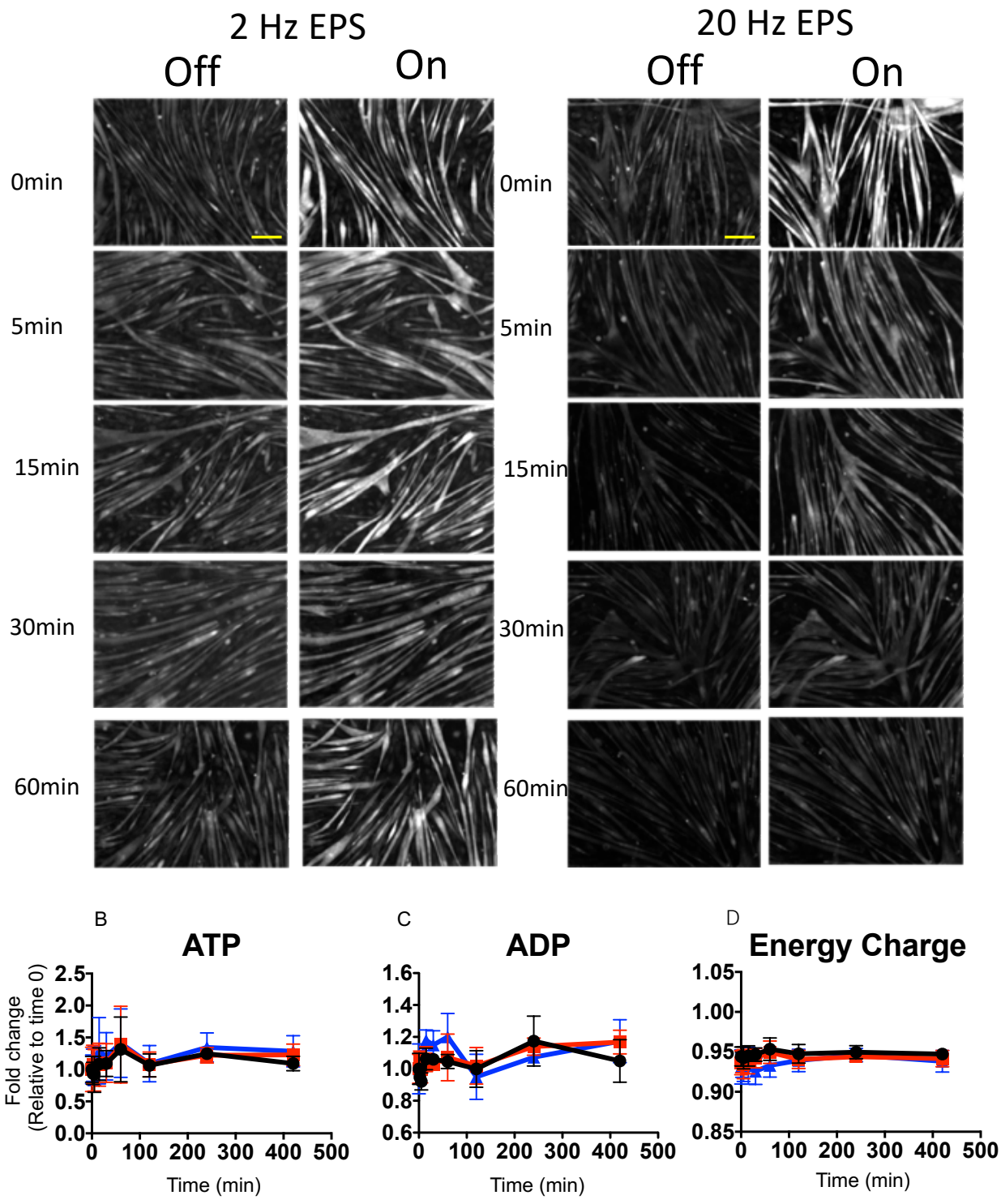

Figure S2 - (A) Images of EPS-induced Ca^{2+} signals in myotubes at 0, 5, 15, 30 and 60 min of 2 Hz or 20 Hz EPS. Scale bar is 150 um. (B) ATP and (C) ADP levels and (D) calculated energy charge ([ATP] + 0.5*[ADP]/[ATP]+[ADP]+[AMP]) during 0, 2 and 20 Hz EPS. Related to Figure 3.

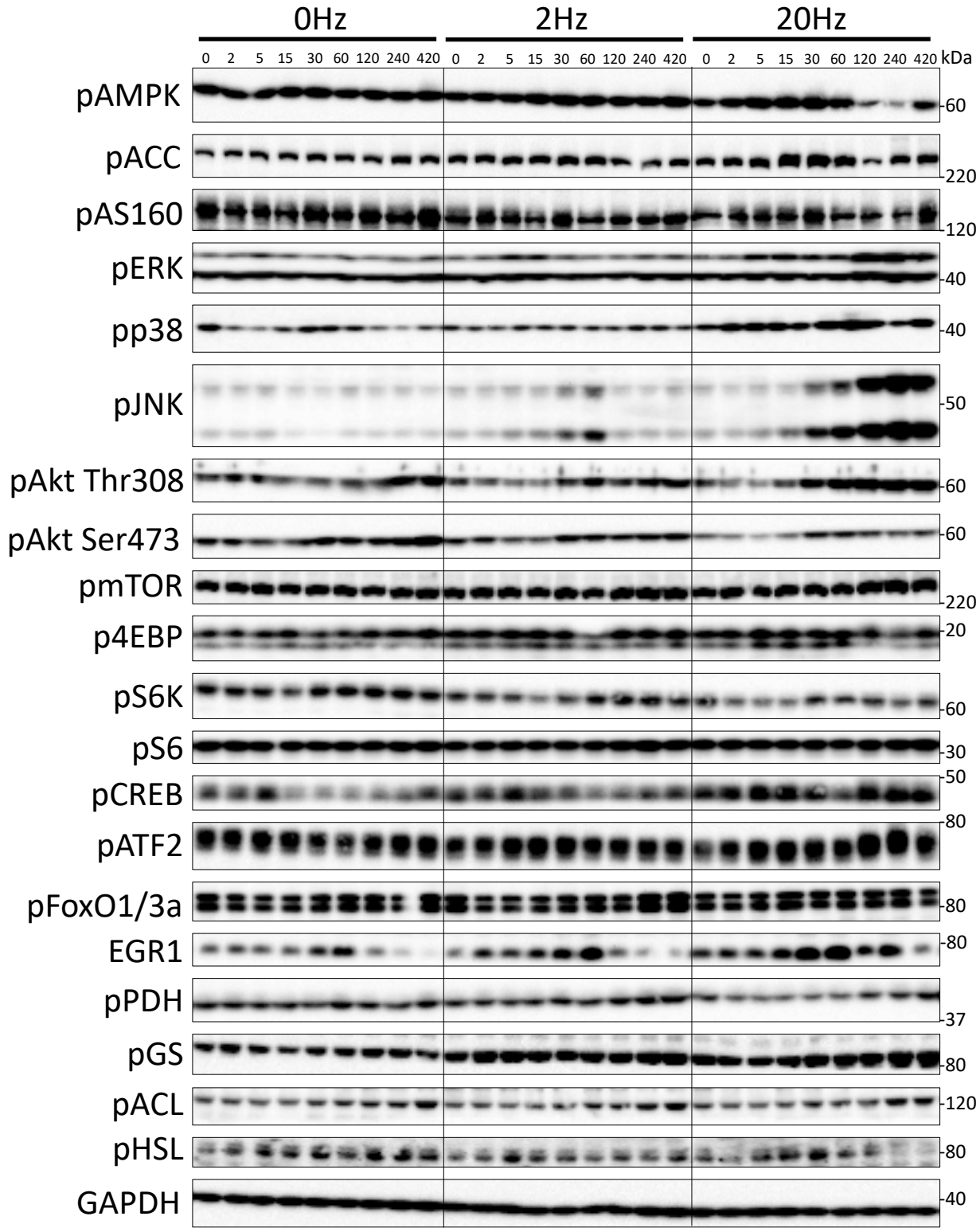

Figure S3 - Representative images of signaling molecules detected by Western blotting. Related to Figure 4.

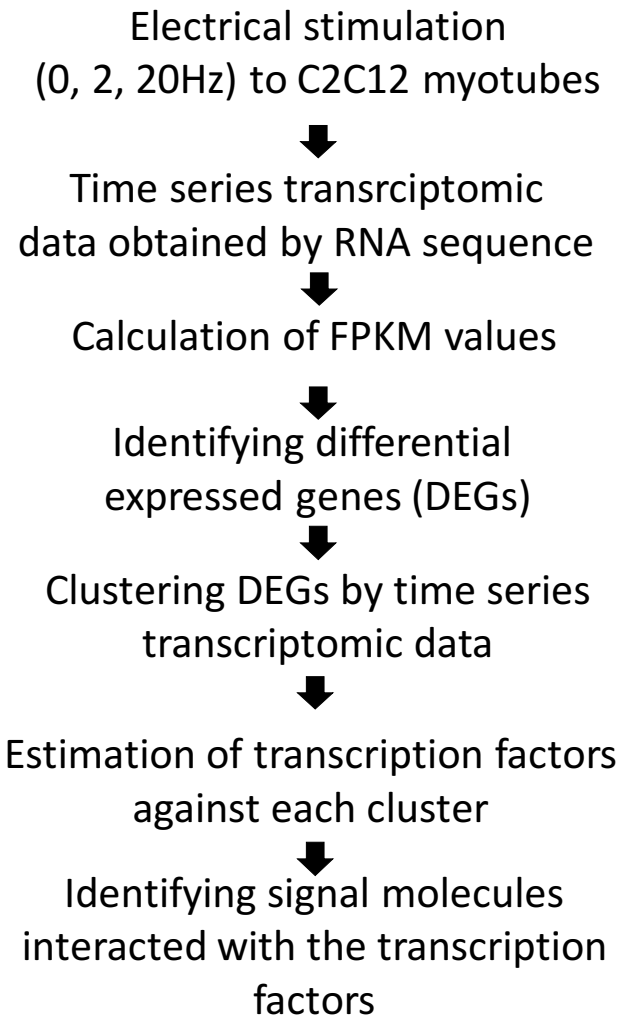

Figure S4 - Analysis of transcriptomic data.

C2C12 myotubes were collected at each time point. RNA sequencing was performed on Hiseq 2500 (Ilumina) (n = 1). Sequencing reads were mapped using TOPHAT v2.0.7, and FPKM values were calculated using Cufflinks. The differentially expressed genes (DEGs) were identified as genes with one or more FPKM values increased or decreased >2.0 fold compared with FPKM at time 0 at 2 Hz or 20 Hz. As a result, 800 genes were identified as DEGs. Hierarchical clustering was performed on these 800 DEGs. TFs were predicted for DEGs in each cluster. Molecules upstream of the predicted TFs were identified as regulators using the KEGG database. Related to Figure 5 and 6.

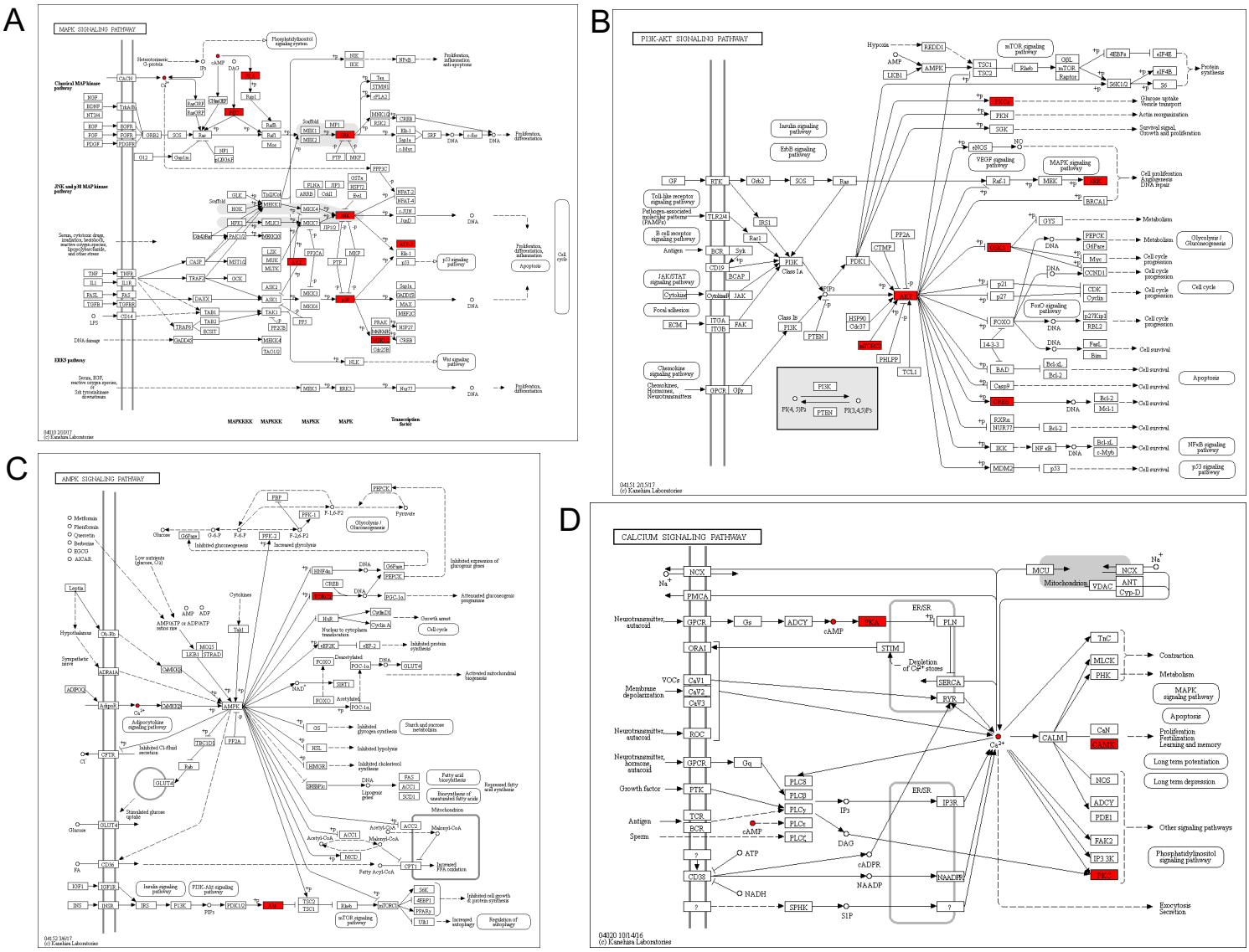

Figure S5 - Identification of regulators upstream of predicted TFs in KEGG signaling pathway map. Related to Figure 6 and 7.

(A) MAPK signaling pathway, (B) PI3-Akt signaling pathway, (C) AMPK signaling pathway, and (D) calcium signaling pathway. Red indicates identified regulators.

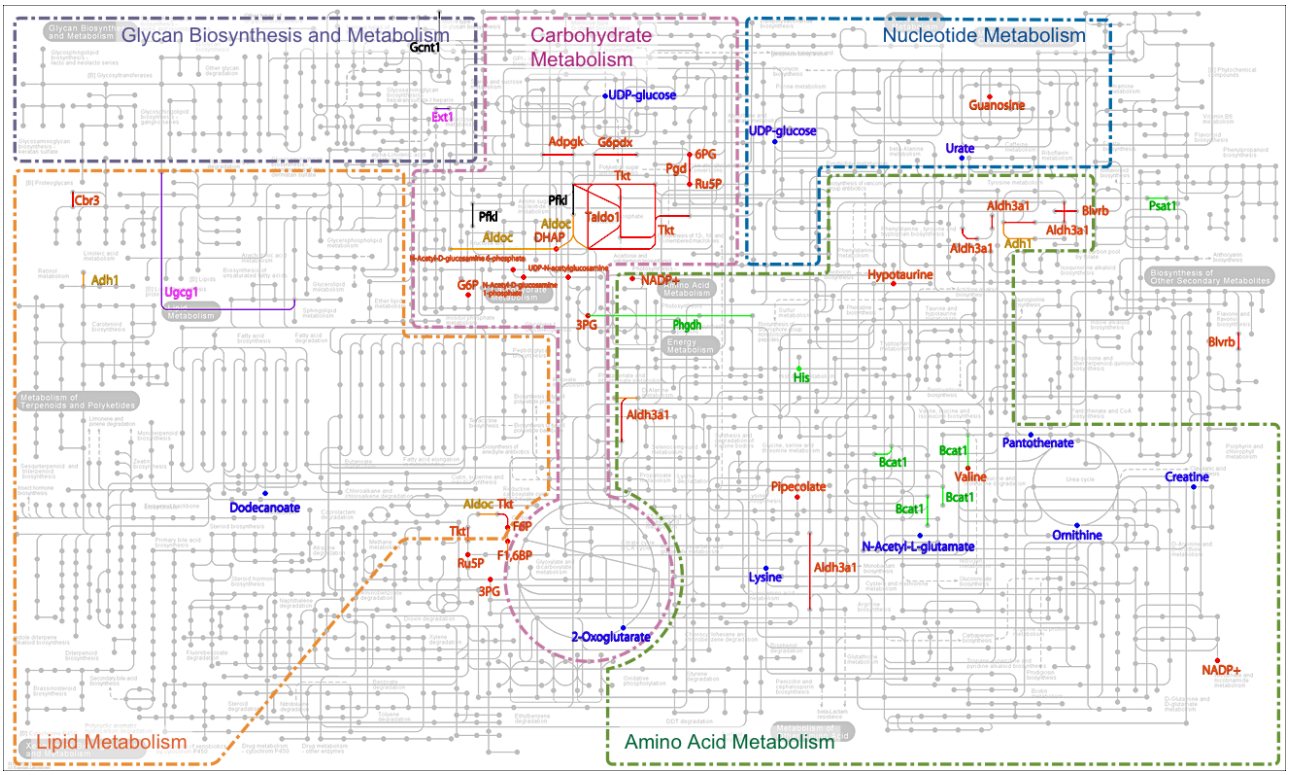

Figure S6 - Identification of significantly changed metabolites and differentially expressed responsible metabolic enzymes. Related to Figure 7.

Red- and blue-colored dots and names indicate metabolites with continuous increase and decrease in levels, respectively. Green-colored dots and names indicate metabolites that both increased and decreased during the time course. Colored lines and names indicate differentially expressed responsible metabolic enzymes in clusters (orange: cluster 1, green: cluster 3, red: cluster 4, blue: cluster 5, purple: cluster 7, black: cluster 8.)

Supplement tables

Table S1. Metabolites in each cluster. Related to Figure 2.

1	2	3	4	5	6	7
Arg	AMP	1-Methylnicotinamide	2-Deoxycytidine	2,3-DPG	1-Methyladenosine	2-Oxoisopentanoate
Argininosuccinate	Adenosine	2-Hydroxyglutarate	4-Acetylbutyrate	2-Hydroxypentanoate	4-Oxopentanoate	2AB
Betaine	Asp	2-Oxoglutarate	5-Methyltetrahydrofolate	3PG	5-Methylthioadenosine	4-Methyl-2-oxopentanoate
Choline	Carnosine	3-Aminoisobutyrate	ADP	5-Aminovalerate	AICAR	5-Oxoproline
Citrulline	Creatine	3-Hydroxy-3-methylglutarate	ATP	6-Phosphogluconate	Adenine	Ala
Glu-Glu	Dodecanoate	3-Methylhistidine	Butanoate	ADP-glucose	Adipate	Asn
Guanidinoacetate	Fumarate	ADMA	CDP-choline	CMP	Allantoin	CDP
N-Acetylleucine	Gly-Leu	Carbamoylaspartate	CTP	CMP-N-acetylneuraminate	Azelate	Dodecanedioate
Phosphorylcholine	Guanosine	Carnitine	Citramalate	Citrate	Citraconate	GABA
	Malate	Creatinine	Cytidine	DHAP	Diethanolamine	Gln
	Pelargonate	Glu	GDP	F1,6P	Glutarate	Gluconate
	Succinate	Glutathione(ox)	GMP	F6P	Glycerate	Glucosamine
	UDP	Glutathione(red)	GTP	FAD	Glycolate	Glucuronate
	UTP	Gly	Hexanoate	G1P	Malonate	Glycerophosphate
	Urate	Gly-Gly	Indole-3-acetate	G3P	Phthalate	His
	beta-Ala-Lys	Glycerophosphorylcholine	N-Methylalanine	G6P	Putrescine(1,4-Butanediamine)	Hydroxyproline
	Pyridoxamine 5-phosphate	Homovanillate	Nicotinamide	GDP-mannose	Terephthalate	Ile
	Proline betaine	Isethionate	O-Phosphoserine	Hypotaurine	UDP-N-acetylglucosamine	Isocitrate
	Methyl sulfate	Lys	SAH	IMP	UDP-glucuronate	Lactate
		N-Acetyl-beta-alanine	Ser	N1-Acetylspermidine	Urea	Leu
		N-Acetylglucosamine	Thymidine	NADP+	o-Acetylcarnitine	Met
		N-Acetylglutamate	UMP	PEP	Acetyl CoA	NADPH
		N-Formylmethionine	Ethanolamine phosphate	PRPP		Ophthalmate
		N-epsilon-Acetyllysine		Pipecolate		Ornithine
		N6,N6,N6-Trimethyllysine		R5P		Phe
		NAD+		Ru5P		Pro
		NADH		S7P		Pyruvate
		Pantothenate		Spermidine		SAM+
		Pyridoxal		Thiamine		Thr
		Pyridoxine		cis-Aconitate		Trp
		S-Lactoylglutathione		gamma-Guanidinobutyrate		Tyr
		Taurine		Ribulose 1,5-diphosphate		Val
		Threonate		N-Acetylglucosamine 1-phosphate		alpha-Aminoadipate
		UDP-glucose		N-Acetylglucosamine 6-phosphate		
		beta-Ala		Methionine sulfoxide		
		gamma-Butyrobetaine				
		glycogen				
		threo-beta-methylaspartate				
		reduced/oxidized glutathione				
		Thiamine monophosphate				

Table S2. Significantly changed metabolites after 20 Hz EPS. Red, blue, and green indicate metabolites that continuously increased, continuously decreased, and both increased and decreased, respectively. Related to Figure 3.

0 Hz vs 2 Hz	0 Hz vs 20 Hz	2 Hz vs 20 Hz
None	G6P	G6P
	F6P	F6P
	F1,6P	F1,6P
	DHAP	DHAP
	3PG	3PG
	2-Oxoglutarate	2-Oxoglutarate
	2-Hydroxyglutarate	2-Hydroxyglutarate
	6-Phosphogluconate	Succinate
	Ru5P	6-Phosphogluconate
	N-Acetyl-beta-alanine	Ru5P
	Urate	N-Acetyl-beta-alanine
	N-Acetylglutamate	Urate
	Dodecanoate	N-Acetylglucosamine 6-phosphate
	Pantothenate	UDP-glucose
	N-Acetylglucosamine 1-phosphate	CMP-N-acetylneuraminate
	N-Acetylglucosamine 6-phosphate	NAD+
	UDP-glucose	Gly
	UDP-N-acetylglucosamine	Ala
	CMP-N-acetylneuraminate	Hypotaurine
	NADP+	5-Aminovalerate
	Hypotaurine	Val
	5-Aminovalerate	Pipecolate
	Val	Ile
	Pipecolate	Gly-Gly
	Creatine	Lys
	Gly-Gly	Methionine sulfoxide
	Ornithine	Phosphorylcholine
	Lys	N6,N6,N6-Trimethyllysine
	His	ADMA
	Methionine sulfoxide	reduced/oxidized glutathione
	Guanosine	
	reduced/oxidized glutathione	

Table S3. Signaling molecules in each cluster. Related to Figure 4.

1	2	3	4
pAkt Ser473	pACL	pAMPK	pp38
pAkt Thr308	pAS160	pACC	pCREB
EGR1	pFoxO1/3a	pHSL	pERK
pGS	pPDH	p4EBP	pATF
pmTOR	pS6K		pJNK
			pS6

Table S4. KEGG pathway analysis of genes enriched in each cluster. Related to Figure 5.

Cluster	Term	Count	P-Value	Benjamini	Genes
1	Fructose and mannose metabolism	2	8.70E-02	8.10E-01	*EGR1, IL6*
	Prion diseases	2	8.20E-02	9.60E-01	*Akr1c13, aldoc*
2	MAPK signaling pathway	6	2.80E-03	1.20E-01	*DDIT3, FOS, DUSP4, DUSP5, Gadd45g, Hspb1*
	p53 signaling pathway	3	2.80E-02	4.80E-01	*Gadd45g, SESN2, mdm2*
3	Glycine, serine and threonine metabolism	3	4.90E-03	1.90E-01	*PHGDH, SHMT2, PSAT1*
	Methane metabolism	2	2.30E-02	2.90E-01	*cat, SHMT2*
	Vitamin B6 metabolism	2	2.00E-02	3.50E-01	*AOX1, PSAT1*
	One carbon pool by folate	2	5.20E-02	4.40E-01	*mthfd2, SHMT2*
4	Glutathione metabolism	10	4.40E-09	4.00E-07	*G6pdx, GCLC, GCLM, gsta1, GSTA4, GSTP1, mgst2, PGD, gstm1, gsr*
	Metabolism of xenobiotics by cytochrome P450	9	6.00E-07	2.70E-05	*adh7, ALDH3A1, CYP1B1, ephX1, gsta1, GSTA4, GSTP1, mgst2, gstm1*
	Drug metabolism	7	1.80E-04	5.50E-03	*adh7, ALDH3A1, gsta1, GSTA4, GSTP1, mgst2, gstm1*
	Pentose phosphate pathway	4	3.00E-03	6.60E-02	*G6pdx, PGD, taldo1, tkt*
	Porphyrin and chlorophyll metabolism	3	4.50E-02	5.70E-01	*BLVRB, FTH1, hmox1*
	Aminoacyl-tRNA biosynthesis	3	8.10E-02	7.20E-01	*AARS, Nars, SARS*
5	Phosphatidylinositol signaling system	3	3.30E-02	9.00E-01	*dgkq, Pik3r1, PIK3C2B*
6	None				
7	Focal adhesion	6	3.30E-03	1.70E-01	*Igf1, Pak3, BCL2, Pdgfb, Thbs1, thbs2*
	Prostate cancer	3	8.00E-02	7.90E-01	*Igf1, BCL2, Pdgfb,*
	TGF-beta signaling pathway	3	7.50E-02	8.90E-01	*INHBA, Thbs1, thbs2,*
8	Cell cycle	8	5.90E-07	2.20E-05	*ttk, BUB1, Cdk1, CCNA2, CCNB2, PTTG1, PLK1, CCNB1*
	Progesterone-mediated oocyte maturation	6	2.20E-05	4.10E-04	*BUB1, Cdk1, CCNA2, CCNB2, PLK1, CCNB1*
	Oocyte meiosis	6	9.30E-05	1.20E-03	*BUB1, Cdk1, CCNB2, PTTG1, PLK1, CCNB1*
	p53 signaling pathway	4	2.80E-03	2.60E-02	*GTSE1, Cdk1, CCNB2, CCNB1*

Table S5. List of differentially changed responsible metabolic enzymes. Cluster numbers are shown in Figure 5. Colors are shown in Figure S6. Related to Figure 5 and 7.

mmu	gene name	cluster number	color
mmu:11522	Adh1	1	orange
mmu:27384	Akr1c13	1	orange
mmu:11676	Aldoc	1	orange
mmu:216188	Aldh1l2	3	green
mmu:12035	Bcat1	3	green
mmu:236539	Phgdh	3	green
mmu:107272	Psat1	3	green
mmu:11529	Adh7	4	red
mmu:72141	Adpgk	4	red
mmu:11670	Aldh3a1	4	red
mmu:233016	Blvrb	4	red
mmu:109857	Cbr3	4	red
mmu:13078	Cyp1b1	4	red
mmu:14381	G6pdx	4	red
mmu:14782	Gsr	4	red
mmu:18104	Nqo1	4	red
mmu:110208	Pgd	4	red
mmu:67103	Ptgr1	4	red
mmu:21351	Taldo1	4	red
mmu:21881	Tkt	4	red
mmu:108155	Ogt	5	blue
mmu:20148	Dhrs3	7	purple
mmu:14042	Ext1	7	purple
mmu:15117	Has2	7	purple
mmu:22234	Ugcg	7	purple
mmu:14537	Gcnt1	8	black
mmu:18641	Pfkl	8	black

Table S6. KEGG pathway analysis of 27 differentially changed responsible metabolic enzymes. Related to Figure 5 and 7.

Rank	Term	number of genes	P-Value	Benjamini
1	Metabolic pathways	18	1.10E-08	4.50E-07
2	Carbon metabolism	9	1.10E-06	2.30E-05
3	Biosynthesis of antibiotics	10	1.50E-06	2.10E-05
4	Pentose phosphate pathway	6	1.20E-05	1.30E-04
5	Biosynthesis of amino acids	7	4.90E-05	4.20E-04
6	Glycolysis / Gluconeogenesis	6	1.00E-04	7.30E-04
7	Metabolism of xenobiotics by cytochrome P450	5	1.00E-02	6.00E-02
8	Retinol metabolism	3	3.40E-02	1.60E-01
9	Tyrosine metabolism	3	3.40E-02	1.60E-01
10	Chemical carcinogenesis	4	6.20E-02	2.60E-01

Table S7. KEGG pathway analysis of the differentially changed responsible metabolic enzymes in cluster 4. Related to Figure 5 and 7.

Rank	Term	number of genes	P-Value	Benjamini
1	Carbon metabolism	5	1.50E-05	1.90E-04
2	Pentose phosphate pathway	4	8.60E-06	2.20E-04
3	Metabolism of xenobiotics by cytochrome P450	4	8.60E-05	7.40E-04
4	Biosynthesis of antibiotics	5	1.60E-04	1.10E-03
5	Metabolic pathways	8	6.00E-04	3.10E-03
6	Glutathione metabolism	3	2.60E-03	1.10E-02
7	Glycolysis / Gluconeogenesis	3	3.80E-03	1.40E-02
8	Chemical carcinogenesis	3	7.20E-03	2.30E-02
9	Tyrosine metabolism	2	5.40E-02	1.50E-01
10	Drug metabolism - cytochrome P450	2	9.00E-02	2.20E-01

Transparent Methods

C2C12 culture

C2C12 myoblasts were seeded into four-well rectangular plates at a density of 3.0×10^5 cells/well, with 3 mL of growth medium comprising Dulbecco's Modified Eagle's Medium (DMEM with 25 mM glucose; Wako, Japan) supplemented with 10% fetal bovine serum. Myoblasts culture was maintained in an incubator at 37°C under a 5% CO_2 atmosphere. After 2 days, the medium was replaced with a differentiation medium consisting of DMEM supplemented with 2% horse serum. Six days after differentiation, cells were used for EPS.

Electrical pulse stimulation (EPS) and N-acetylcysteine (NAC) treatment

EPS was performed using the method of Manabe et al. (Manabe et al., 2012). Briefly, differentiated C2C12 myotubes were used 16 h after the final change of medium. The four-well plates were connected to the electrical stimulation apparatus, a four-well C-Dish (Ion Optix Corp., Milton, MA, USA), and myotubes were stimulated by electric pulses generated by an electrical pulse generator (Uchida Denshi, Hachioji, Japan). Myotubes were stimulated with electric pulses of 50 V at 0, 2, or 20 Hz for 3 ms for a given time period in an incubator at 37°C. We used 2 Hz for low frequency and 20 Hz for high frequency stimulation. Previous studies confirmed that 20 Hz was high frequency for C2C12 myotubes (Fujita et al., 2007; Yamasaki et al., 2009) but 20 Hz is not considered high frequency stimulation for skeletal muscle *in vivo* (Cairns et al., 2007). To inhibit the accumulation of ROS, we added NAC (5 mM) after 1 h of 20 Hz EPS and collected cells 3 h after the EPS.

Metabolome Analysis

The stimulated cells were washed twice with 5% mannitol and incubated for 10 min in 1 mL methanol containing 25 μM each of the three internal standards [L-methionine sulphone (Wako), D-camphor-10-sulphonic acid (Dojindo, Kumamoto, Japan), and 2-(N-morpholin-o)ethanesulfonic acid (Wako)]. After 500 uL Milli-Q purified water was added, 600 uL of the solution was taken and mixed well with 400 uL chloroform and then centrifuged for 15 min at 20,000 g and 4°C. The separated 400 uL aqueous layer was centrifugally filtered through a 5 kDa cutoff filter (Millipore, Burlington, MA, USA) to remove residual protein. The filtrate (320 μL) was lyophilized and dissolved in 50 uL Milli-Q water containing reference compounds [200 μM each of trimesate (Wako) and 3-aminopyrrolidine (Sigma-Aldrich, St. Louis, MO, USA)] and then injected into a CE-TOF-MS system (Agilent Technologies, Santa Clara, CA, USA) (Soga et al., 2006, 2009). We performed independent biological triplicates and excluded metabolites that could not be measured in any of the three samples. For data analysis, the obtained

absolute concentration (μM) in the suspension was normalized to that at time 0 to generate relative values.

Glycogen content assay

Glycogen content was quantified using the method of Noguchi et al. (Noguchi et al., 2013). The cell suspension was incubated for 1 h with 1.2 mL of 30% (w/v) KOH solution at 95°C; 61.2 uL of glacial acetic acid and 1% (w/v) linear polyacrylamide were added to 200 uL of the cell suspension to coprecipitate glycogen. Then 400 uL pure ethanol was added to the mixture to precipitate the total glycogen and the mixture was centrifuged for 15 min at 15,000 r.p.m. at 4°C. The supernatants were discarded, and the pellets were resuspended in 50 uL of 50 mM NaOAc buffer (comprising an equal volume of 50 mM sodium acetate and 50 mM acetate). Then 600 uL pure ethanol was added to the resuspended sample. The resuspended sample was centrifuged for 15 min at 15,000 r.p.m. at 4°C. After the supernatant was discarded, the pellet was dried to eliminate any residual ethanol and incubated with 20 uL amyloglucosidase (0.1 mg/mL in 50 mM NaOAc buffer) for 2 h at 55°C. After the incubation, hydrolyzed glycogen was measured using the glucose assay.

Intracellular calcium ion (Ca^{2+}) measurement

C2C12 myotubes were washed twice with phosphate buffered saline (PBS). Ca^{2+} assay buffer, comprising Fluo-8 dye loading solution (AAT Bioquest Inc., Sunnyvale, CA, USA) and DMEM cell medium without serum, was added to the wells and incubated at 37°C for 30 min. Myotubes were stimulated with electric pulses at 2 Hz or 20 Hz in the incubator and observed at the indicated time under an inverted fluorescence microscope, IX 83 (Olympus, Tokyo, Japan) 755 equipped with a UPLSAPO10X2 objective lens (Olympus) an ORCA-R2 C10600-10B CCD camera (Hamamatsu Photonics, Shizuoka, Japan) , a U-HGLGPS mercury lamp (Molecular Devices, San Jose, CA, USA), a U-FBNA mirror unit (Olympus), an MD XY30100T-META automatically programmable stage position (Molecular Devices.).

Western blotting

Total proteins were extracted from cells by 50 mM Tris-Cl pH 7.5 with 2% SDS at the indicated time points after EPS and subjected to standard SDS-PAGE. The resolved proteins were transferred to nitrocellulose membranes and probed with specific antibodies (antibodies against pAKT [Ser473, #9271, Thr308, #9275], pAMPK [Thr172, #2535], pACC [Ser89, #3661], pAS160 [Thr642, #4288], pERK [Thr202/Tyr204, #9101], pp38 [Thr180/Tyr182, #9211], pS6K [Thr389, #9205], p4EBP [Thr37/46, #2855], pCREB [Ser133, #9198], pJNK [Thr183/Tyr185, #4668], pmTOR [Ser2488, #2971], pATF2

[Thr71, #9221], pACL [Ser455, #4331], pFoxo1/3a [Thr24/Thr32, #9464], pHSL [Ser563, #4139], pGS [Ser641, #3891], EGR1 [#4154], and GAPDH [#2118] were purchased from Cell Signaling Technology Japan (Tokyo, Japan); antibody against pPDH [Ser293, ab92696] was purchased from Abcam (Cambridge, UK). The signal was visualized using chemiluminescence and horseradish peroxidase (HRP)-conjugated secondary antibodies (GE Healthcare, Chicago, IL, USA) and the Immobilon Western Chemiluminescent HRP Substrate (Millipore) using a LAS4000 imager (Fujifilm, Tokyo, Japan). The intensities of the specific bands were quantified using TotalLab TL120 (Nonlinear Dynamics) analysis software. Quantitative values were normalized using GAPDH quantities as standards.

RNA Sequencing

Total RNA was extracted from C2C12 myotubes at 0, 1, 3, and 6 h after 0, 2, or 20 Hz EPS using RNeasy Mini Kit (Qiagen, Hilden, Germany). mRNA was enriched from total RNA using poly(A) selection, and quality of the mRNA samples was validated using 2100 Bioanalyzer (Agilent). RNA integrity number (RIN) values were a range of 8.9-9.7 across samples. Standard Illumina protocols were used to generate 101-base pair, paired-end sequencing reads on the HiSeq 2500 platform (Illumina, San Diego, CA, USA) (Matsumoto et al., 2014). Q30, which is an index of sequence quality, was 86-88% and sequencing depth was more than 50.0 million reads across samples. The sequence data are deposited to DDBJ (Accession number DRA010400).

Identification of differentially expressed genes

The obtained sequencing reads were aligned to the reference mouse genome sequence GRCm38 (Ensemble release 75), using TopHat v2.0.7 (Trapnell et al., 2009). Mapping rate using TOPHAT across samples was 74-79%. FPKM values were calculated using Cufflinks (Trapnell et al., 2010). We removed genes with FPKM < 1 at all time points based on results from a previous RNA-seq study (Väremo et al., 2015). The DEGs were identified as genes with FPKM values that changed more than 2.0-fold and less than 0.5-fold compared with those at time 0 at more than one time point under 2 and/or 20 Hz.

Hierarchical clustering

We performed hierarchical clustering analysis by Ward method using MATLAB (Mathworks) (Sano et al., 2016). For normalization, L2 normalization was performed for each time series data of metabolites, signal molecules, and transcripts.

TF prediction using Motif Enrichment Analysis

We performed motif enrichment analysis following CIDER methods (Mina et al., 2015) to determine enrichment of TF binding motifs in promoter region [−300 bp to +100 bp flanking the consensus transcription start site (Arner et al., 2015; Kinsella et al., 2011)] of DEGs in each cluster. Binding sites of each TF were determined using sequences obtained from Ensembl BioMart (Kinsella et al., 2011), TRANSFAC Pro (Matys et al., 2006), and the Match tool (Kel et al., 2003). We used extended vertebrate_non_redundant_min_SUM.prf, one of the parameter sets prepared in TRANSFAC Pro for the threshold of similarity score calculated by Match. The enrichment of TF binding motifs in the promoter of DEGs in each cluster was determined by Fisher's exact test with FDR following Storey's procedure (Storey et al., 2004). The TFs predicted from the significantly enriched TF binding motifs (FDR < 0.01) were identified as the TFs regulating DEGs in each cluster.

Identification of regulators of TFs

Using the accession numbers from TRANSFAC, we associated the significantly enriched TF binding motifs with TFs using the identifiers obtained from matrix.dat in TRANSFAC Pro. The accession numbers of TFs provided in TRANSFAC Pro are associated with the gene IDs in DATF, EMBL, FLYBASE, MIRBASE, PATHODB, PDB, SMARTDB, SWISSPROT, TRANSCOMPEL, or TRANSPATH. To identify regulators of the TFs, the gene IDs from EMBL, PDB, or SWISSPROT that were associated with the accession numbers of human, mouse, and rat TF were converted to KEGG gene IDs using bioDBnet (https://biodbnet-abcc.ncifcrf.gov/) (Mudunuri et al., 2009). We manually determined the upstream regulators of the TFs from the four signaling pathways (MAPK signaling, PI3K-AKT signaling, calcium signaling, and AMPK signaling) based on KEGG.

Identification of responsible metabolic enzymes that were differentially expressed

To identify responsible metabolic enzymes that were differentially expressed, metabolic enzymes with quantitatively changed metabolites as substrates or products were extracted from KEGG database. Among these metabolic enzymes, those encoded by the DEGs were defined as differentially expressed responsible metabolic enzymes.

KEGG pathway analysis

We used the DAVID tool (https://david.ncifcrf.gov/home.jsp) (Huang et al., 2008, 2009) for KEGG pathway analysis.

Statistical analysis

For identification of quantitatively changed metabolites, comparison of the mean concentration of metabolites under 0, 2, and 20 Hz EPS at each time point was performed using Welch's t-test. P values were adjusted for multiple testing with the Storey's procedure (Storey et al., 2004) using MATLAB (Mathworks) function *mafdr* for time points during (0, 2, 5, 15, 30, and 60 min) and after (120, 240, and 420 min) EPS, and the adjusted p values are shown as q values. When $q < 0.2$ at two or more time points, the metabolite was defined as a quantitatively changed metabolite. Statistical comparison of the level of each molecule among 0, 2, and 20 Hz at each time point was performed using two-way ANOVA. The calculated p value for the electrical stimulation was corrected for multiple testing using the Benjamini–Hochberg method, and $q < 0.1$ was regarded as a significant difference.

Supplemental references

Arner, E., Daub, C.O., Vitting-Seerup, K., Andersson, R., Lilje, B., Drablos, F., Lennartsson, A., Ronnerblad, M., Hrydziuszko, O., Vitezic, M., et al. (2015). Transcribed enhancers lead waves of coordinated transcription in transitioning mammalian cells. Science (80-.). *347*, 1010–1014.

Cairns, S.P., Chin, E.R., and Renaud, J.-M. (2007). Stimulation pulse characteristics and electrode configuration determine site of excitation in isolated mammalian skeletal muscle: implications for fatigue. J. Appl. Physiol. *103*, 359–368.

Fujita, H., Nedachi, T., and Kanzaki, M. (2007). Accelerated de novo sarcomere assembly by electric pulse stimulation in C2C12 myotubes. Exp. Cell Res. *313*, 1853–1865.

Huang, D.W., Sherman, B.T., and Lempicki, R.A. (2008). Systematic and integrative analysis of large gene lists using DAVID bioinformatics resources. Nat. Protoc. *4*, 44–57.

Huang, D.W., Sherman, B.T., and Lempicki, R.A. (2009). Bioinformatics enrichment tools: paths toward the comprehensive functional analysis of large gene lists. Nucleic Acids Res. *37*, 1–13.

Kel, A.E., Gössling, E., Reuter, I., Cheremushkin, E., Kel-Margoulis, O. V, and Wingender, E. (2003). MATCH: A tool for searching transcription factor binding sites in DNA sequences. Nucleic Acids Res. *31*, 3576–3579.

Kinsella, R.J., Kahari, A., Haider, S., Zamora, J., Proctor, G., Spudich, G., Almeida-King, J., Staines, D., Derwent, P., Kerhornou, A., et al. (2011). Ensembl BioMarts: a hub for data retrieval across taxonomic space. Database *2011*, bar030.

Manabe, Y., Miyatake, S., Takagi, M., Nakamura, M., Okeda, A., Nakano, T., Hirshman, M.F., Goodyear, L.J., and Fujii, N.L. (2012). Characterization of an Acute Muscle Contraction Model Using Cultured C2C12 Myotubes. PLoS One *7*. e52592.

Matsumoto, K., Suzuki, A., Wakaguri, H., Sugano, S., and Suzuki, Y. (2014). Construction of mate pair full-length cDNAs libraries and characterization of transcriptional start sites and termination sites. Nucleic Acids Res. *42*, e125–e125.

Matys, V., Kel-Margoulis, O. V., Fricke, E., Liebich, I., Land, S., Barre-Dirrie, A., Reuter, I., Chekmenev, D., Krull, M., Hornischer, K., et al. (2006). TRANSFAC(R) and its module TRANSCompel(R): transcriptional gene regulation in eukaryotes. Nucleic Acids Res. *34*, D108–D110.

Mina, M., Magi, S., Jurman, G., Itoh, M., Kawaji, H., Lassmann, T., Arner, E., Forrest, A.R.R., Carninci, P., Hayashizaki, Y., et al. (2015). Promoter-level expression clustering identifies time development of transcriptional regulatory cascades initiated by ErbB receptors in breast cancer cells. Sci. Rep. *5*, 11999.

Mudunuri, U., Che, A., Yi, M., and Stephens, R.M. (2009). bioDBnet: the biological database network. Bioinformatics *25*, 555–556.

Noguchi, R., Kubota, H., Yugi, K., Toyoshima, Y., Komori, Y., Soga, T., and Kuroda, S. (2013). The selective control of glycolysis, gluconeogenesis and glycogenesis by temporal insulin patterns. Mol. Syst. Biol. *9*, 664.

Sano, T., Kawata, K., Ohno, S., Yugi, K., Kakuda, H., Kubota, H., Uda, S., Fujii, M., Kunida, K., Hoshino, D., et al. (2016). Selective control of up-regulated and down-regulated genes by temporal patterns and doses of insulin. *112*, 1–12.

Soga, T., Baran, R., Suematsu, M., Ueno, Y., Ikeda, S., Sakurakawa, T., Kakazu, Y., Ishikawa, T., Robert, M., Nishioka, T., et al. (2006). Differential metabolomics reveals ophthalmic acid as an oxidative stress biomarker indicating hepatic glutathione consumption. J. Biol. Chem. *281*, 16768–16776.

Soga, T., Igarashi, K., Ito, C., Mizobuchi, K., Zimmermann, H.-P., and Tomita, M. (2009). Metabolomic Profiling of Anionic Metabolites by Capillary Electrophoresis Mass Spectrometry. Anal. Chem. *81*, 6165–6174.

Storey, J.D., Taylor, J.E., and Siegmund, D. (2004). Strong control, conservative point estimation and simultaneous conservative consistency of false discovery rates: a unified approach. J. R. Stat. Soc. Ser. B (Statistical Methodol). *66*, 187–205.

Trapnell, C., Pachter, L., and Salzberg, S.L. (2009). TopHat: discovering splice junctions with RNA-Seq. Bioinformatics *25*, 1105–1111.

Trapnell, C., Williams, B.A., Pertea, G., Mortazavi, A., Kwan, G., van Baren, M.J., Salzberg, S.L., Wold, B.J., and Pachter, L. (2010). Transcript assembly and quantification by RNA-Seq reveals unannotated transcripts and isoform switching during cell differentiation. Nat. Biotechnol. *28*, 511–

515.

Väremo, L., Scheele, C., Broholm, C., Mardinoglu, A., Kampf, C., Asplund, A., Nookaew, I., Uhlén, M., Pedersen, B.K., and Nielsen, J. (2015). Proteome- and Transcriptome-Driven Reconstruction of the Human Myocyte Metabolic Network and Its Use for Identification of Markers for Diabetes. Cell Rep. *11*, 921–933.

Yamasaki, K.I., Hayashi, H., Nishiyama, K., Kobayashi, H., Uto, S., Kondo, H., Hashimoto, S., and Fujisato, T. (2009). Control of myotube contraction using electrical pulse stimulation for bio-actuator. J. Artif. Organs *12*, 131–137.